IEEE Access
Multidisciplinary ⋮ Rapid Review ⋮ Open Access Journal

Received July 10, 2021, accepted July 18, 2021, date of publication July 20, 2021, date of current version July 28, 2021.

Digital Object Identifier 10.1109/ACCESS.2021.3098800

Trajectory Tracking of a Novel Underactuated AUV via Nonsingular Integral Terminal Sliding Mode Control

ZHIWEI WU, HAOSONG PENG, BIAO HU, AND XIAODONG FENG

College of Information Science and Technology, Beijing University of Chemical Technology, Beijing 100029, China

Corresponding author: Haosong Peng (livion_i@icloud.com)

This work was supported by the National Natural Science Foundation of China under Grant 91848103.

ABSTRACT This paper addresses the 3D trajectory tracking problem of a novel underactuated underwater vehicle with 4 propellers. A 5-DOF kinematic and dynamic model of the quadrotor underwater vehicle (QUV) is established based on the underwater vehicle and quadrotor unmanned aerial vehicle movement mechanism. A double-loop control structure is then developed. By constructing a Lyapunov function for the outer-loop controller, a 5-DOF trajectory tracking error equation and a velocity virtual control law are obtained. The inner-loop controller is built based on nonsingular integral terminal sliding mode control (NITSMC). Finally, the effectiveness and robustness of our control algorithm are demonstrated through numerical simulations. In particular, given a smooth, second-order derivable 3D reference trajectory, the QUV can quickly track the trajectory and satisfactorily converges in the neighborhood of the expected value in a finite time via NTISMC, which verifies its superiority compared with the other popular backstepping control (BSC) method.

INDEX TERMS AUV, trajectory tracking control, nonsingular integral terminal sliding mode control.

I. INTRODUCTION

Autonomous underwater vehicles (AUVs) were developed more than 60 years ago. AUVs carry power independently, can perform a wide range of detections, and have been widely used in marine scientific research, marine engineering operations, and national defense and military fields. To save energy consumption and reduce underwater resistance, many AUV designs are submarine-like [1]–[3]. An AUV is a type of insufficient DOF underwater vehicle that lacks the ability to move in the roll, sway and vertical directions. AUVs are unable to complete the practical applications of wall-sticking motion and one-DOF depth control. To solve the motion defects of AUVs and simultaneously reduce their power consumption and water resistance, an AUV imitating a quadrotor UAV is proposed, which is generally called a QUV. The quadrotor makes full use of the coupling relationship between the four propellers to achieve 6-DOF motion. Combining its propeller design with AUV, a new AUV model [4]–[7] is obtained. However, due to its underactuated characteristics, the modeling and control of QUV are very difficult. The commonly used method is to adjust the placement angle of the propellers in order to obtain thrust in other directions, which changes the characteristics of the underactuated motion of the quadrotor and only achieves vertical motion without combining the coupling dynamic equation of the AUV. In fact, the traditional AUV can easily derive the 5-DOF error equation by using the simplified coordinate transformation equation when performing trajectory tracking motion control. However, due to the particularity of the QUV activity angle, many mathematical operations are required to derive the QUV's 5-DOF error equation, which makes it difficult to research QUV and greatly limits the systematic construction of the QUV. To solve the abovementioned problems, this paper proposes a new QUV model in section II by combining the quadrotor drone model and the kinematic and dynamic model of AUVs, which decouples the dynamic equation and achieves a high efficiency in controlling the AUV's motion.

To verify the correctness of the QUV model and the QUV's movement capability, 3D trajectory tracking of the QUV is simulated. The 3D trajectory tracking problem has always been a critical issue in the control of underwater vehicles.

The associate editor coordinating the review of this manuscript and approving it for publication was Jiajia Jiang.

Lapierre and Pascoal [8], [9] proposed a nonlinear control strategy that globally converges trajectory tracking error. Strict proof-of-error convergence was also proposed. In terms of control methods, Do and Jie [10] decomposed the desired trajectory to obtain the virtual control law, and the backstepping method was used to design the actual control law. Repoulias [11] was aimed at 2D trajectory tracking motion, using the geometric relationship between the expected velocity in the S-F coordinate system and the coordinates of underwater vehicles to obtain the expected (angular) velocity with a controller by solving complex differential equations. Then, the backstepping method was used to design the actual control law. Li *et al.* [12] extended Repoulias' method to 3D space and designed an integral sliding mode controller to solve the 3D trajectory control problem. Jiang *et al.* [13] designed a Lyapunov function to stabilize the tracking error and proved that the derivative of the Lyapunov function is negative definite. The virtual control law simplifies the design of the actual control law. Bioinspired computing was then utilized to replace the derivative of the virtual control law, and they proposed integral sliding mode control. The control methods of underwater vehicles also include PID control and adaptive fuzzy control [14], [15], with new methods constantly being proposed. Additionally, some nonideal situations during trajectory tracking, such as obstacle avoidance or controller thrust saturation, have also been extensively studied in recent years [16]–[18].

Although there are various control methods for underwater vehicles, these methods are based on the traditional AUV model, and very few studies have been conducted on 3D trajectory tracking with the QUV model. The roll angle ϕ can be ignored when the AUV model performs coordinate transformation, which simplifies the transformation matrix. However, due to the particularity of QUV motion, the roll angle ϕ is nonignorable, which makes the coordinate transformation more complicated. To address this problem, in Section III, we propose a tracking error model of QUV and derive a virtual control law. In addition, we also apply the NITSMC method to stabilize the trajectory tracking error. The simulation results show that 3D trajectory tracking control results with the tracking error model in this paper are consistent with the actual motion of the quadrotor. Moreover, it shows that the NITSMC method is superior to the backstepping control method in terms of control.

After a careful literature review, we find that some challenging problems are still worth studying. First, how to control a 5-DOF QUV is not studied well. Previous studies focus much attention on the problem of trajectory tracking of traditional AUV model, while a few researches pay attention to systematizing QUV modeling. How to make them follow our desired trajectory timely and accurately needs to be further studied. Second, there are many advanced control structures and approaches at present. However, how to apply them to control a 5-DOF QUV model proposed in this paper is still not clear. Thus, it is necessary to study the performance in controlling a 5-DOF QUV to track a 3D trajectory, for the aim of enriching the research scope of QUV controllers.

Regarding the above problems, this article proposes an advanced controller to solve the 3D trajectory tracking problem for a novel underactuated AUV. The main contributions of this article are listed as follows.

1) Establishing the kinematic and dynamic model of QUV and proposing a 5-DOF error equation.
2) A double-loop control system with nonsingular integral terminal sliding mode control is designed for QUV.
3) Simulations of 3D trajectory tracking of QUV verify the accuracy of the model and the superiority of the control method.

The remainder of this paper can be described as follows: Section IV proves the stability of the virtual control law and proves the stability of NITSMC. The convergent time of NITSMC is briefly analyzed. In section V, the simulation of 3D trajectory tracking via the NISTMC method is conducted and compared with the BSC method.

II. MODELING A QUADROTOR UNDERWATER VEHICLE

The design concept of the QUV model draws on the motion principle of the quadrotor UAV. This section will begin with coordinate transformation based on the Euler angle and establish the kinematic model and dynamic model of the QUV based on underwater vehicle modeling theory by Thor I. Fossen [19], [20]. Finally, 5-DOF kinematic and dynamic equations for the motion of the QUV are proposed.

A. THE PRINCIPLE OF QUV MOVEMENT

As shown in Fig. 1, M1, M2, M3, and M4 are four underwater propellers that generate propelling forces F_1, F_2, F_3, and F_4, respectively. Motors M2 and M4 on the two diagonals rotate counterclockwise, and M1 and M3 rotate clockwise to generate the lift force and the reverse torque. Symmetrical installation can offset the reverse torque. The QUV movement includes the following parts.

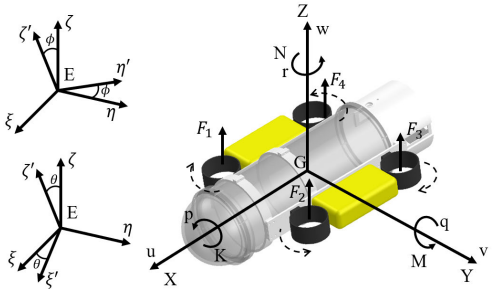

FIGURE 1. Configuration of a quadrotor AUV.

1) ROLL, PITCH AND YAW

By increasing the speed of M3 and M4 by the same amount while reducing the speed of M1 and M2, the lift behind is greater than the lift in front, and the QUV pitches forward. Similarly, by reducing the speed of M1 and M4 by the same

amount and increasing the speed of M2 and M3 by the same amount, the QUV will roll to the right; otherwise, by increasing the speed of M1 and M4 while reducing the speed of M2 and M3, the QUV will roll to the left.

By increasing the speed of M2 and M4 by the same amount while reducing the speed of M1 and M3 by the same amount, the clockwise torque will increase, which makes the QUV yaw clockwise. At this time, the total lift has not changed, and there will be no vertical movement. In the same way, it can achieve counterclockwise horizontal yaw motion.

2) SURGE, SWAY, AND HEAVE

Increasing the speed of all propellers, the QUV will float up while the sum of lift and buoyancy is greater than gravity; otherwise, it will dive. Let the QUV perform roll and pitch motions to produce an angle with the horizontal plane first, and then increase the speed of all propellers. The component force of the resultant force on the horizontal plane is utilized to complete the sway and surge.

The principle of the QUV movement indicates that the yaw motion of the QUV is relatively independent and unnecessary. To simplify the model, the underwater vehicle discussed in this paper will not consider yaw motion.

B. KINEMATIC MODEL

The earth frame $E-\xi\eta\zeta$ and underwater vehicle body frame $G-xzy$ used in this paper are marked as shown in Fig. 1. The body-frame (angular) velocity $\boldsymbol{\nu}$ can be translated into the inertial (angular) velocity $\dot{\boldsymbol{\eta}}$ by the following kinematic equations [20]

$$\dot{\boldsymbol{\eta}} = \boldsymbol{J}(\boldsymbol{\eta})\boldsymbol{\nu} \tag{1}$$

where

$$\boldsymbol{J}(\boldsymbol{\eta}) = \begin{bmatrix} \boldsymbol{J_1}(\boldsymbol{\eta_1}) & \boldsymbol{0_{3\times3}} \\ \boldsymbol{0_{3\times3}} & \boldsymbol{J_2}(\boldsymbol{\eta_2}) \end{bmatrix} \tag{2}$$

With $\boldsymbol{\eta} = [\boldsymbol{\eta_1}, \boldsymbol{\eta_2}]^\top$, $\boldsymbol{\eta_1} = [\xi, \eta, \zeta]^\top$, $\boldsymbol{\eta_2} = [\phi, \theta, \psi]^\top$, $\boldsymbol{\nu} = [\boldsymbol{\nu_1}, \boldsymbol{\nu_2}]^\top$, $\boldsymbol{\nu_1} = [u, v, w]^\top$, $\boldsymbol{\nu_2} = [p, q, r]^\top$.

ξ, η, and ζ are the positions of surge, sway, and heave in the earth frame, and ϕ, θ, and ψ are the roll angle, pitch angle and yaw angle, respectively. u, v, and w are the linear velocities of QUV in the X, Y, and Z directions on the body frame, and p, q, and r are the angular velocities of the QUV in the K, M, and N directions on the body frame.

For linear velocities, the conversion matrix $\boldsymbol{J_1}$ from the body frame to the earth frame is given by

$$\boldsymbol{J_1}(\boldsymbol{\eta_1}) = \begin{bmatrix} c\psi c\theta & -s\psi c\phi + c\psi s\phi s\theta & s\phi s\psi + c\psi s\theta c\phi \\ s\psi c\theta & c\phi c\psi + s\phi s\theta s\psi & -s\phi c\psi + c\phi s\theta s\psi \\ -s\theta & c\theta s\phi & c\theta c\phi \end{bmatrix} \tag{3}$$

where c, s and t denote $cos(\cdot)$, $sin(\cdot)$ and $tan(\cdot)$ in this paper, respectively.

For angular velocities, the conversion matrix $\boldsymbol{J_2}$ from the body frame to the earth frame is given by

$$\boldsymbol{J_2}(\boldsymbol{\eta_2}) = \begin{bmatrix} 1 & s\phi t\theta & c\phi t\theta \\ 0 & c\phi & -s\phi \\ 0 & s\phi/c\theta & c\phi/c\theta \end{bmatrix} \tag{4}$$

Considering the movement of QUV in reality, ϕ is required to satisfy $|\phi| < \pi/2$, and to avoid singular values, θ is required to satisfy $|\theta| < \pi/2$. Substituting formulas (2), (3), and (4) into formula (1) and ignoring ψ, the kinematic model with 5 DOFs can be obtained as

$$\begin{cases} \dot{\xi} = uc\theta + vs\phi s\theta + wc\phi s\theta \\ \dot{\eta} = vc\phi - ws\phi \\ \dot{\zeta} = -us\theta + vcs\phi + wc\phi c\theta \\ \dot{\phi} = p + qs\phi t\theta \\ \dot{\theta} = qc\phi \end{cases} \tag{5}$$

Remark 1: The difference between the 5-DOF equations of QUV and traditional AUVs is the angle of rotation. QUV relies on the θ angle and the ϕ angle to generate the surge and sway motion components, which makes the kinematic equation more complicated than the traditional AUV.

C. DYNAMIC MODEL

The 6-DOF model of the underwater vehicle can be described by the following nonlinear kinematic equation.

$$\boldsymbol{M}\dot{\boldsymbol{\nu}} + \boldsymbol{C}(\boldsymbol{\nu})\boldsymbol{\nu} + \boldsymbol{D}(\boldsymbol{\nu})\boldsymbol{\nu} + \boldsymbol{g}(\boldsymbol{\eta}) = \boldsymbol{\tau} \tag{6}$$

where $\boldsymbol{M} = \boldsymbol{M}_{RB} + \boldsymbol{M}_A$; $\boldsymbol{C}_v = \boldsymbol{C}_{RB} + \boldsymbol{C}_A$; $\boldsymbol{M}_{RB}$ is the rigid-body system inertia matrix; $\boldsymbol{M}_A$ is a 6×6 system inertia matrix of the added mass terms; $\boldsymbol{C}_{RB}$ is the rigid-body Coriolis and centripetal matrix; $\boldsymbol{C}_A$ is the added mass coefficient for underwater vehicles; $\boldsymbol{D}$ is the total hydrodynamic damping matrix; and the vector $\boldsymbol{\tau}$ represents the propulsion forces and moments. These parameter matrices can be calculated or estimated as follows:

The notations of SNAME(1950) are used in the dynamic model of QUV, which are summarized in Tab. 1.

TABLE 1. Notations and descriptions.

Notation	Description	Unit
m	Mass of the QUV	kg
B	Buoyancy of the QUV	N
z_B	Center of buoyancy in Z direction	m
I_x, I_y, I_z	Momentum of Inertia in the X, Y, Z directions	kg/m^2
$X_{\dot{u}}, Y_{\dot{v}}, Z_{\dot{w}}$	Added mass terms in the X, Y, Z directions	kg
$K_{\dot{p}}, M_{\dot{q}}, N_{\dot{r}}$	Added mass terms in the K, M, N directions	kg/m^2
X_u, Y_v, Z_w	Linear damping terms in the X, Y, Z directions	kg/s
K_p, M_q, N_r	Linear damping terms in the K, M, N directions	m^2/s

1) INERTIA MATRIX

The QUV uses four propellers as the main power, which are deployed symmetrically on both sides of the body. Due to the characteristics of this structure, the vehicle is approximately

symmetrical about the $x-y$, $x-z$, and $y-z$ planes in the body frame.

The inertial matrix $\boldsymbol{M}$ includes the hydrodynamic add mass matrix $\boldsymbol{M}_A$ and the rigid-body system inertia matrix M_{RB}, which are defined as

$$\boldsymbol{M}_{RB} = \begin{bmatrix} m\boldsymbol{I}_{3\times3} & \boldsymbol{0}_{3\times3} \\ \boldsymbol{0}_{3\times3} & \boldsymbol{I}_c \end{bmatrix} \tag{7}$$

where $\boldsymbol{I}_c = \text{diag}\left(I_x, I_y, I_z\right)$ and I_x, I_y, I_z are inertia moments.

$$\boldsymbol{M_A} = -\text{diag}\left(X_{\dot{u}}, Y_{\dot{v}}, Z_{\dot{w}}, K_{\dot{p}}, M_{\dot{q}}, N_{\dot{r}}\right) \tag{8}$$

2) CORIOLIS AND THE ADDED MASS MATRIX

The Coriolis-centripetal matrix $\boldsymbol{C}$ includes a rigid-body Coriolis and centripetal matrix $\boldsymbol{C}_{RB}$ and a hydrodynamic Coriolis and centripetal matrix $\boldsymbol{C}_A$. When QUV is allowed to move only at a low speed, $\boldsymbol{C}_A$ can simply be described as

$$\boldsymbol{C}_A(\boldsymbol{v}) = \begin{bmatrix} 0 & 0 & 0 & 0 & -Z_{\dot{w}}w & Y_{\dot{v}}v \\ 0 & 0 & 0 & Z_{\dot{w}}w & 0 & -X_{\dot{u}}u \\ 0 & 0 & 0 & -Y_{\dot{v}}v & X_{\dot{u}}u & 0 \\ 0 & -Z_{\dot{w}}w & Y_{\dot{v}}v & 0 & -N_{\dot{r}}r & M_{\dot{q}}q \\ Z_{\dot{w}}w & 0 & -X_{\dot{u}}u & N_{\dot{r}}r & 0 & -K_{\dot{p}}p \\ -Y_{\dot{v}}v & X_{\dot{u}}u & 0 & -M_{\dot{q}}q & K_{\dot{p}}p & 0 \end{bmatrix} \tag{9}$$

Assuming that the center of gravity coordinates coincide with the origin of the buoyancy coordinate, the rigid-body Coriolis and centripetal matrix $\boldsymbol{C}_{RB}$ can simply be represented as follows:

$$\boldsymbol{C}_{RB}(\boldsymbol{v}) = \begin{bmatrix} 0 & 0 & 0 & 0 & mw & -mv \\ 0 & 0 & 0 & -mw & 0 & mu \\ 0 & 0 & 0 & mv & -mu & 0 \\ 0 & mw & -mv & 0 & I_z r & -I_y q \\ -mw & 0 & mu & -I_z r & 0 & I_x p \\ mv & -mu & 0 & I_y q & -I_x p & 0 \end{bmatrix} \tag{10}$$

When the QUV is considered to have three symmetry planes, only the linear uncoupled damping term should be considered

3) HYDRODYNAMIC DAMPING MATRIX

The QUV is considered to have three symmetry planes, so to simplify the modeling, only the linear uncoupled damping term should be considered.

$$\boldsymbol{D}(\boldsymbol{v}) = -\text{diag}\left\{X_u, Y_v, Z_w, K_p, M_q, N_r\right\} \tag{11}$$

4) STATIC

The static force $\boldsymbol{g}(\boldsymbol{\eta})$ refers to the combined force of the moment of gravity (W) and buoyancy (B) on the QUV. In the actual design of an underwater vehicle, the origin of the body frame is taken as the center of gravity of the vehicle, and the center of buoyancy is slightly higher than gravity, i.e., the actual position of the center of gravity in the body frame is [0, 0, 0], the actual position of the buoyancy center is [0, 0, z_B], and then the static force of the QUV is

$$\boldsymbol{g}(\boldsymbol{\eta}) = \begin{bmatrix} -(B-W)s_\theta \\ (B-W)c\theta s\phi \\ -(B-W)c\theta c\phi \\ z_B B s\phi c\theta \\ z_B B s\theta \\ 0 \end{bmatrix} \tag{12}$$

5) THRUST

The calculation formula of the thrust and thrust moment is as follows [21]:

$$\boldsymbol{\tau} = \left[0, 0, U_1, U_2, U_3, 0\right]^\top \tag{13}$$

where U_1 is the total lift produced by the four propellers, which is proportional to the square of the speed under ideal conditions, and U_2 and U_3 are the moments produced by the propellers in the K and M directions of the body frame. Their specific definition is

$$\begin{bmatrix} U_1 \\ U_2 \\ U_3 \end{bmatrix} = \begin{bmatrix} C_T\left(\Omega_1^2 + \Omega_2^2 + \Omega_3^2 + \Omega_4^2\right) \\ -\frac{\sqrt{2}b}{2}C_T\left(\Omega_1^2 - {\Omega_2}^2 - {\Omega_3}^2 + {\Omega_4}^2\right) \\ -\frac{\sqrt{2}b}{2}C_T\left({\Omega_1}^2 + {\Omega_2}^2 - {\Omega_3}^2 - {\Omega_4}^2\right) \end{bmatrix} \tag{14}$$

where $\Omega_i (i = 1, 2, 3, 4)$ is the speed of propellers M1-M4, b is the torque length, and C_T is the lift coefficient of the propeller. It can be seen from formula (14) that increasing Ω_2 and Ω_3 will boost the thrust U_2 and the QUV will roll to the left, which meets the principle of QUV movement.

Substituting formulas (7), (8), (9), (10), (11), (12) and (13) into formula (6), the simplified 5-DOF dynamic model that ignored yaw motion can be obtained:

$$\begin{cases} 0 = -(m - X_{\dot{u}})\dot{u} + X_u u - (m - Z_{\dot{w}})qw - s\theta(B - W) \\ 0 = -(m - Y_{\dot{v}})\dot{v} + Y_v v + (m - Z_{\dot{w}})pw + c\theta s\phi(B - W) \\ U_1 = (m - Z_{\dot{w}})\dot{w} - Z_w w - (m - X_{\dot{u}})qu + (m - Y_v)pv \\ \quad -c\phi c\theta(B - W) \\ U_2 = (I_x - K_{\dot{p}})\dot{p} - K_p p + (Y_{\dot{v}} - Z_{\dot{w}})vw + Bz_B c\theta s\phi \\ U_3 = (I_y - M_{\dot{q}})\dot{q} - M_q q - (X_{\dot{u}} - Z_{\dot{w}})uw + Bz_B s\theta \end{cases} \tag{15}$$

III. 3D TRAJECTORY TRACKING ON A QUADROTOR UNDERWATER VEHICLE

In this section, 3D trajectory tracking of the QUV is discussed. In the first part, tracking error equations for the QUV are established, and the Lyapunov function is designed to obtain the virtual control law of angular velocity. The second part uses NITSMC to gradually converge the tracking error. The trajectory studied in this paper is time-varying, and to avoid singular values when reverse solving the expected angular velocity, the trajectory must be a continuous and smooth 3D curve that has a second time derivative.

Note that the subscript d and the subscript e are used to represent the expected value and the tracking error, respectively. The superscript B is used to represent the body frame.

A. ESTABLISHMENT OF THE 3D TRJECTORY TRACKING ERROR EQUATION

The movement mechanism of the QUV is similar to that of a quadrotor, where the relatively independent yaw angle ψ can be ignored. Let the coordinates of any point on a continuous trajectory curve in 3D space be (ξ_d, η_d, ζ_d). Similarly, let the expected angle be (ϕ_d, θ_d). The expected velocity is the time derivative of the coordinates, which can be expressed as $(\dot{\xi_d}, \dot{\eta_d}, \dot{\zeta_d})$. Clearly, $w_d = \sqrt{\dot{\xi}_d^2 + \dot{\eta}_d^2 + \dot{\zeta}_d^2}$, $u_d = 0$, and $v_d = 0$. According to the geometric relationship, the desired angle can be expressed by the desired velocity. Hence, $\theta_d = \arctan(\dot{\xi_d}/\dot{\zeta_d})$ and $\phi_d = -\arctan(\dot{\eta_d}/\sqrt{\dot{\xi}_d^2 + \dot{\zeta}_d^2})$.

According to the conversion relationship (5) between the angular velocity and angle, combined with the derivative of the desired angle, the expression of the desired angular velocity p_d and q_d can be listed as

$$\begin{cases} \dot{\phi}_d = \dfrac{\dot{\eta}_d(\ddot{\xi}_d + \ddot{\zeta}_d) - \ddot{\eta}_d(\dot{\xi}_d^2 + \dot{\zeta}_d^2)}{\sqrt{\dot{\xi}_d^2 + \dot{\zeta}_d^2}(\dot{\xi}_d^2 + \dot{\eta}_d^2 + \dot{\zeta}_d^2)} \\ \dot{\theta}_d = \dfrac{\ddot{\xi}_d\dot{\zeta}_d - \dot{\xi}_d\ddot{\zeta}_d}{\dot{\xi}_d^2 + \dot{\zeta}_d^2} \\ q_d = \dfrac{\dot{\theta}_d}{c\phi_d} \\ p_d = \dot{\phi}_d - q_d s\phi_d t\theta_d \end{cases} \tag{16}$$

At moment t, the tracking errors of the 5-DOF in the earth frame are denoted as

$$\begin{aligned} &\xi_e = \xi - \xi_d \quad \eta_e = \eta - \eta_d \quad \zeta_e = \zeta - \zeta_d \\ &\phi_e = \phi - \phi_d \quad \theta_e = \theta - \theta_d \end{aligned}$$

Apparently, the velocity error and angular velocity error in the earth frame can be written as

$$\dot{\boldsymbol{\eta}}_e = \boldsymbol{J}(\boldsymbol{\eta})\boldsymbol{v} - \boldsymbol{J_d}(\boldsymbol{\eta})\boldsymbol{v_d} \tag{17}$$

To simplify the calculation of the virtual control law, transfer the tracking errors from the earth frame to the body frame

$$\begin{bmatrix} \xi_e^B \\ \eta_e^B \\ \zeta_e^B \end{bmatrix} = \boldsymbol{J_1^{-1}}(\boldsymbol{\eta_1}) \begin{bmatrix} \xi_e \\ \eta_e \\ \zeta_e \end{bmatrix} \tag{18}$$

Since the transition matrix is a nonsingular orthogonal matrix, the stabilization is still equivalent after the conversion. Taking the time derivative of tracking errors (18) in the body frame, we can deduce that

$$\begin{aligned} \begin{bmatrix} \dot{\xi}_e^B \\ \dot{\eta}_e^B \\ \dot{\zeta}_e^B \end{bmatrix} &= \dot{\boldsymbol{J}}_1^{-1}(\boldsymbol{\eta_1}) \begin{bmatrix} \xi_e \\ \eta_e \\ \zeta_e \end{bmatrix} + \boldsymbol{J_1}^{-1}(\boldsymbol{\eta_1}) \begin{bmatrix} \dot{\xi}_e \\ \dot{\eta}_e \\ \dot{\zeta}_e \end{bmatrix} \\ &= \left(\dot{\phi} \frac{\partial \boldsymbol{J_1}^{-1}(\boldsymbol{\eta_1})}{\partial \phi} + \dot{\theta} \frac{\partial \boldsymbol{J_1}^{-1}(\boldsymbol{\eta_1})}{\partial \theta} \right) \begin{bmatrix} \xi_e \\ \eta_e \\ \zeta_e \end{bmatrix} \\ &\quad + \boldsymbol{J_1}^{-1}(\boldsymbol{\eta_1}) \left(\boldsymbol{J_1}(\boldsymbol{\eta_1})\boldsymbol{v_1} - \boldsymbol{J_{1d}}(\boldsymbol{\eta_1})\boldsymbol{v_{1d}} \right) \\ &= \left(\dot{\phi} \frac{\partial \boldsymbol{J_1}^{-1}(\boldsymbol{\eta_1})}{\partial \phi} + \dot{\theta} \frac{\partial \boldsymbol{J_1}^{-1}(\boldsymbol{\eta_1})}{\partial \theta} \right) \boldsymbol{J_1}(\boldsymbol{\eta_1}) \begin{bmatrix} \xi_e^B \\ \eta_e^B \\ \zeta_e^B \end{bmatrix} \\ &\quad + \boldsymbol{v_1} - \boldsymbol{J_1}^{-1}(\boldsymbol{\eta_1})\boldsymbol{J_{1d}}(\boldsymbol{\eta_1})\boldsymbol{v_{1d}} \end{aligned} \tag{19}$$

Substituting the error transition (18) and angular velocity (3) into (19), the 5-DOF tracking error equations are expressed as

$$\begin{cases} \dot{\xi}_e^B = u + w_d c\phi_d s\theta_e - qc\phi s\phi\eta_e^B + qc^2\phi\zeta_e^B \\ \dot{\eta}_e^B = v - w_d\,(c\phi_d s\phi c\theta_e - c\phi s\phi_d) \\ \qquad\quad +(p + qs\phi t\theta)\zeta_e^B + qs\phi c\phi\xi_e^B \\ \dot{\zeta}_e^B = w - w_d\,(c\phi_d c\phi c\theta_e + s\phi s\phi_d) \\ \qquad\quad +qc^2\phi\xi_e^B - (p + qs\phi t\theta)\,\eta_e^B \\ \dot{\phi}_e = p_e + qs\phi t\theta - q_d s\phi_d t\theta_d \\ \dot{\theta}_e = qc\phi - q_d c\phi_d \end{cases} \tag{20}$$

Since the pitch angle and roll angle are meaningless in the body frame, it is unnecessary to transfer the angle to the body frame. Therefore, the critical situation of trajectory tracking is letting (20) gradually converge in a finite time. If ε is defined as the asymptotically stable range in the sense of Lyapunov, then convergence of the tracking error can be expressed as

$$\begin{aligned} &\lim_{t\to\infty} |\xi_e^B| < \varepsilon \quad \lim_{t\to\infty} |\eta_e^B| < \varepsilon \quad \lim_{t\to\infty} |\zeta_e^B| < \varepsilon \\ &\lim_{t\to\infty} |\phi_e| < \varepsilon \quad \lim_{t\to\infty} |\theta_e| < \varepsilon \end{aligned} \tag{21}$$

Obviously, trajectory tracking errors will be stabilized when (21) is satisfied.

B. DESIGN OF THE CONTROL LAW BASED ON INTEGRAL TERMINAL SLIDING MODE

The sliding mode control method and backstepping control method are commonly used to stabilize the tracking errors (21). However, designing a sliding mode surface of the tracking errors will complicate the actual control law. A simple Lyapunov function proposed by Jiang *et al.* can stabilize the tracking errors and simplify the actual control law.

Setting the Lyapunov function as follows

$$V = \frac{1}{2}(\xi_e^B)^2 + \frac{1}{2}(\eta_e^B)^2 + \frac{1}{2}(\zeta_e^B)^2 + 1 - c\phi_e + 1 - c\theta_e \tag{22}$$

Taking the time derivative of V and substituting (20) into the derivative of V yields

$$\begin{aligned} \dot{V} &= \xi_e^B\dot{\xi}_e^B + \eta_e^B\dot{\eta}_e^B + \zeta_e^B\dot{\zeta}_e^B + \dot{\phi}_e s\phi_e + \dot{\theta}_e s\theta_e \\ &= \xi_e^B(u + w_d c\phi_d s\theta_e) \\ &\quad +\eta_e^B(v + w_d c\phi s\phi_d - w_d c\phi_d s\phi c\theta_e) \\ &\quad +\zeta_e^B(w - w_d s\phi s\phi_d - w_d c\phi c\phi_d c\theta_e) \\ &\quad +s\phi_e(p - p_d + qs\phi t\theta - q_d s\phi_d t\theta_d) \\ &\quad +s\theta_e(qc\phi - q_d c\phi_d) \end{aligned}$$

$$
\begin{aligned}
&= \xi_e^B u + \eta_e^B \left(v + w_d c\phi s\phi_d (1 - c\theta_e)\right) \\
&\quad + \zeta_e^B (w - w_d s\phi s\phi s\phi_d - w_d c\phi c\phi_d c\theta_e) \\
&\quad + s\phi_e (p - p_d + qs\phi t\theta - q_d s\phi_d t\theta_d - w_d c\theta_e \eta_e^B) \\
&\quad + s\theta_e (qc\phi - q_d c\phi_d + w_d c\phi_d \xi_e^B) \qquad (23)
\end{aligned}
$$

Introduce ξ_e^B and η_e^B into virtual control laws α_p and α_q. Let the derivative of V be negative definite, so the designed virtual control law can be written as

$$
\begin{aligned}
\alpha_w &= w_d (s\phi s\phi_d + c\phi c\phi_d c\theta_e) - k_1 \zeta_e^B \\
\alpha_p &= p_d - qs\phi t\theta + q_d s\phi_d t\theta_d + w_d c\theta_e \eta_e^B - k_2 s\phi_e \\
\alpha_q &= (q_d c\phi_d - w_d c\phi_d \xi_e^B - k_3 s\theta_e)/c\phi \qquad (24)
\end{aligned}
$$

where $k_1, k_2, k_3 > 0$ are undesigned control parameters.

When ξ_e^B, η_e^B, ζ_e^B, ϕ_e and θ_e converge to zero, QUV follows the trajectory. Although we designed the virtual control law of w, p, q, these variables are not directly controllable. Therefore, the tracking error stabilization problem is now transformed into a properly designed actual control law to track the virtual control law with a high control quality. The efficiency and robustness of sliding mode control in nonlinear systems can converge the deviation of the actual control law and the virtual control law. For a first-order controlled object, integral sliding mode control with an integral (ISMC) error is generally used to improve the control quality. The integral sliding mode can make the system only have a sliding stage by obtaining a suitable initial position, which also ensures robustness, but the convergence time might tend to be infinite. Nonsingular terminal sliding mode control (NTSMC) can ensure that the system state converges to zero in a finite amount of time. In addition, its dynamic performance is better than ordinary sliding mode control [22]. The NITSMC method, which combines the two control methods, can achieve convergence in a limited amount of time and improve the control quality. The following designs a nonsingular integral terminal sliding surface first. Then, the actual control law is designed via the NITSMC method, and the stability and convergence time are analyzed.

To establish the NITSMC model, the error and integral error between the actual control law and the virtual control law are defined.

$$
\begin{aligned}
e_{w1} &= \int_0^t e_{w2} \mathrm{d}t \quad e_{p1} = \int_0^t e_{p2} \mathrm{d}t \; e_{q1} = \int_0^t e_{q2} \mathrm{d}t \\
e_{w2} &= w - \alpha_w \quad e_{p2} = p - \alpha_p \; e_{q2} = q - \alpha_q \qquad (25)
\end{aligned}
$$

The sliding surface of the NITSMC presented in [22] is defined as

$$
\begin{bmatrix} s_1 \\ s_2 \\ s_3 \end{bmatrix} = \begin{bmatrix} e_{w1} + \dfrac{1}{\beta_1} e_{w2}^{a_1/b_1} \operatorname{sgn}(e_{w2}) \\ e_{p1} + \dfrac{1}{\beta_2} e_{p2}^{a_2/b_2} \operatorname{sgn}(e_{p2}) \\ e_{q1} + \dfrac{1}{\beta_3} e_{q2}^{a_3/b_3} \operatorname{sgn}(e_{q2}) \end{bmatrix} \qquad (26)
$$

where β_i, a_i, b_i are undesigned control parameters, and $\beta_i > 0$, a_i and b_i are both positive odd numbers that satisfy $a_i > b_i$ and $1 < a_i/b_i < 2$.

Let the Lyapunov function of NITSMC be $V_s = \frac{1}{2}\boldsymbol{s}^\top \boldsymbol{s}$, where the time derivative of V_s is

$$
\dot{V}_s = \boldsymbol{s}^\top \dot{\boldsymbol{s}} = \boldsymbol{s}^\top \left(\dot{\boldsymbol{e}}_1 + \frac{1}{\beta} \frac{a}{b} \boldsymbol{e}_2^{a/b-1} \dot{\boldsymbol{e}}_2 \right) \qquad (27)
$$

To let V_s be negative definite, substituting 5-DOF derivative equations (15) and (26) into (27), the actual control law can be defined as

$$
\begin{aligned}
U_1 &= (m - Z_{\dot{w}}) \left(\dot{\alpha}_w - \beta_1 \frac{b_1}{a_1} e_{w2}^{2-a_1/b_1} - h_1 \operatorname{sgn}(s_1) \right) \\
&\quad - Z_w w - (m - X_{\dot{u}}) qu + (m - Y_v) pv - (B - W) c\phi c\theta \\
U_2 &= (I_x - K_{\dot{p}}) \left(\dot{\alpha}_p - \beta_2 \frac{b_2}{a_2} e_{p2}^{2-a_2/b_2} - h_2 \operatorname{sgn}(s_2) \right) \\
&\quad - K_p p + (Y_{\dot{v}} - Z_{\dot{w}}) vw + B z_B c\theta s\phi \\
U_3 &= (I_y - M_{\dot{q}}) \left(\dot{\alpha}_q - \beta_3 \frac{b_3}{a_3} e_{q2}^{2-a_3/b_3} - h_3 \operatorname{sgn}(s_3) \right) \\
&\quad - M_q q + (Z_{\dot{w}} - X_{\dot{u}}) uw + B z_B s\theta \qquad (28)
\end{aligned}
$$

where $h_i (i = 1, 2, 3)$ represents the speed at the moving point of the system approaching the sliding mode switching surface. Setting $h_i (i = 1, 2, 3)$ larger can obtain a faster approach speed but can also more easily cause control chattering. Note that $0 < 2 - a/b < 1$, which limits $e_2^{(2-a/b)}$ from yielding a singular value.

Furthermore, the derivative of the virtual control law is introduced in (28), which will cause a derivative explosion when deriving the virtual control law. This can be avoided by replacing a low-pass filter with the derivative of the virtual control law. In the sliding mode control system, an ideal sliding mode is formed by introducing the sgn(·) function as an ideal switching function that constantly causes chattering. By introducing the saturation function sat(·) instead of sgn(·), chattering can be either avoided or weakened.

The expression of the saturation function sat(·) is

$$
\operatorname{sat}(s) = \begin{cases} 1 & s > \Delta \\ s/\Delta & |s| \le \Delta \\ -1 & s < -\Delta \end{cases} \qquad (29)
$$

where Δ is the boundary size of the saturation function. A schematic diagram of the proposed overall control system for the QUV is shown in Fig. 2.

Remark 2: As shown in Fig. 2, the QUV control system can be composed of inner loop control and the outer loop control. The inner loop control system stabilizes the actual (angular) velocity to achieve the virtual (angular) velocity via NITSMC, while the outer loop control reversely solves the virtual control law according to the given trajectory and realizes the 3D trajectory tracking of the QUV.

C. STABILITY ANALYSIS

In this section, the stability of the Lyapunov function that derives the virtual control law, and the actual control law are proven.

The pivotal condition for the global convergence of the tracking error is that the derivative of the Lyapunov function

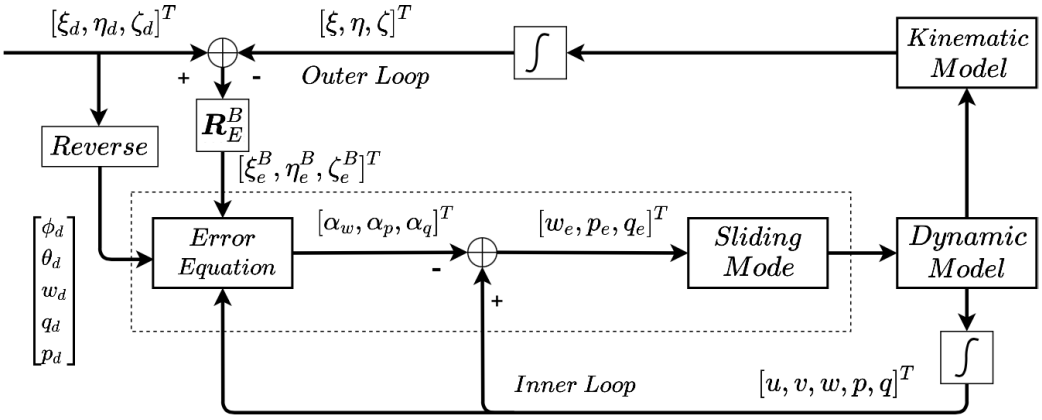

FIGURE 2. Schematic diagram of the control system for QUV.

that derives the virtual control law is negative definite. Substituting the virtual control law (24) into (19) yields

$$\dot{V} = \xi_e^B u + \eta_e^B \left(v + w_d c\phi s\phi_d (1 - c\theta_e)\right) - k_1 \left(\zeta_e^B\right)^2 - k_2 s^2 \phi_e - k_3 s^2 \theta_e \quad (30)$$

Considering a certain situation in which $|c\theta_e| \leq 1$, we can deduce that $\left(\xi_e^B u + \eta_e^B \left(v + w_d c\phi s\phi_d (1 - c\theta_e)\right)\right) \leq |\xi_e^B u + \eta_e^B (v + 2w_d)|$. The derivative of V satisfies the following:

$$\dot{V} \leq -k_1 \left(\zeta_e^B\right)^2 - k_2 s^2 \phi_e - k_3 s^2 \theta_e + |\xi_e^B u + \eta_e^B (v + 2w_d)| \quad (31)$$

The negative definite condition of (31) is related to the undetermined formula $|\xi_e^B u + \eta_e^B (v + 2w_d)|$. The following proves that this undetermined formula is bounded.

Lemma 1: Jiang, Y The surge velocity u, the sway velocity v and the heave velocity w are all bounded.

Jiang, Y. designed a Lyapunov function of v to prove that v is bounded. It can be concluded that u, w are bounded in the same way. For a given smooth curve, w_d is absolutely bounded. Obviously, ξ_e^B and ζ_e^B are also bounded while setting a reasonable starting position, which reveals the undetermined formula $|\xi_e^B u + \eta_e^B (v + 2w_d)| \leq \mathrm{M}$, where M is its upper bound. By selecting the appropriate parameters k_1, k_2, k_3 satisfying $k_1 \left(\zeta_e^B\right)^2 + k_2 s^2 \phi_e + k_3 s^2 \theta_e \geq \mathrm{M}$, Lyapunov is negative definite. Finally, according to *Lyapunov Stability Theory*, the 5-DOF tracking error is asymptotically convergent.

For the stability of the Lyapunov function (27), substituting (26) into (27) yields (32), as shown at the bottom of the next page.

Combined with the actual control law (28),

$$\begin{aligned}\dot{V}_s &= \sum_{i=1}^{3} s_i \left\{ e_2 + \frac{1}{\beta_i} \frac{a_i}{b_i} e_2^{a_i/b_i - 1} \times \left(- \beta_i \frac{b_i}{a_i} e_2^{2 - a_i/b_i} - h_i \operatorname{sgn}(s_i) \right) \right\} \\ &= \sum_{i=1}^{3} s_i \frac{1}{\beta_i} \frac{a_i}{b_i} e_2^{a_i/b_i - 1} \left(- h_i \operatorname{sgn}(s_i) \right) \\ &= - \sum_{i=1}^{3} h_i \frac{1}{\beta_i} \frac{a_i}{b_i} e_2^{a_i/b_i - 1} |s_i| = - \sum_{i=1}^{3} h_i' |s_i| \leq 0 \end{aligned} \quad (33)$$

where $h_i' = h_i \frac{1}{\beta_i} \frac{a_i}{b_i} e_2^{a_i/b_i - 1} (i = 1, 2, 3)$. Because h_i, β_i, a_i, b_i $(i = 1, 2, 3)$ are all positive numbers, $h_i' > 0$ $(i = 1, 2, 3$ *and* $e_2 \neq 0)$. Therefore, $\dot{V}_s \leq 0$, which means $s \equiv 0$ when $\dot{V}_s \equiv 0$. According to the *Lasalle Invariance Principle*, we have $s \to 0$ when $t \to \infty$. Then, according to the *Terminal Sliding Model Properties* [23], when $t \to \infty$, $e \to 0$. Finally, the control law satisfies the Lyapunov stability condition as long as $e_2 \neq 0$.

The convergence time of NITSMC is related to its parameters. Assume the time from $s(0) \neq 0$ to $s(t_r) = 0$ is t_r. Considering a general case where $\dot{V}_s = s\dot{s} = -h|s|$, we have

$$\dot{s} = -\frac{h'|s|}{s} = \pm h' \quad (34)$$

The integration of t from 0 to t_r can be calculated as

$$\int_{s=s(0)}^{s=s(t_r)} ds = \int_{t=0}^{t=t_r} \pm h' \mathrm{d}t \quad (35)$$

Namely, we can deduce that $s(t_r) - s(0) = \pm h' t_r$. The time at which the sliding surface converges to zero can be written as $t_r = |s(0)|/h'$. Assume that the time from $x(t_r) \neq 0$ to $x(t_r + t_s) = 0$ is t_s. The sliding surface s therefore equals 0, while $t \in (t_r, t_s)$, which means $-\beta e_1 = \dot{e}_1^{a/b}$. The integration of t from t_r to $t_r + t_s$ can be calculated as

$$\int_{e_1(t_r)}^{0} (-\beta e_1)^{(-b/a)} \mathrm{d}e_1 = \int_{t_r}^{t_r + t_s} \mathrm{d}t \quad (36)$$

Therefore, the convergent time can be written as

$$t_s = \frac{a}{\beta^{b/a}(a - b)} e_1(t_r)^{1 - b/a} \quad (37)$$

Remark 3: The control object adopting this controller can approach the trajectory faster by setting appropriate parameters. It can be seen from (37) that if $b/a \to 1$ or $\beta \to 0$,

then $t_s \to \infty$. Therefore, we should not set b/a close to 1 or β close to 0.

IV. SIMULATION OF TRAJECTORY TRACKING BASED ON NITSMC

In this section, a series of numerical simulation experiments will be conducted to verify the effectiveness and feasibility of the QUV control method. The detailed QUV model parameters are selected from references [24], [25] [26] and shown in Table 2. The simulation experiments are divided into two categories: one is one-dimensional depth control, and the other is three-dimensional curves composed of sin(.) and cos(.) functions. The units of all variables in this paper use SI.

A. DEPTH CONTROL

Compared with traditional AUVs that use vertical rudders to move in the ζ direction [11], the underwater vehicle designed in this paper has advantages in terms of depth control. The traditional submarine underwater vehicle has no independent actuator in the vertical direction, so it needs the assistance of the vertical rudder; therefore, the coupling velocity in the horizontal direction is inevitably generated. In our model, the four propellers can generate vertical upward or downward thrust independently, without generating velocity and angular velocity in other DOFs, which dramatically simplifies the difficulty in terms of depth control.

The trajectory of the vehicle must be a second-order derivable, so the tanh(·) function is used instead of the step function. The desired position for the QUV in the ζ direction is as follows, with the purposes of verifying the universality and versatility of the controller in the lower dimension and highlighting the movement advantages of our QUV model.

$$\zeta_d = \begin{cases} 5\tanh(100t) & 0 \le 5s \\ 5\tanh(100(t-5))+5 & 5 < t \le 10s \\ -15\tanh(100(t-10))+10 & 10 < t \le 15s \\ 5\tanh(100\,(t-15))-5 & 15 < t \le 20s \end{cases} \tag{38}$$

The initial motion states of QUV are $u_0 = 0(m/s)$, $v_0 = 0(m/s)$, $w_0 = 0(m/s)$, $p_0 = 0(rad/s)$ and $q_0 = 0(rad/s)$. The initial position and angle are $z_0 = 0(m)$, $\phi_0 = 0(rad)$ and $\theta_0 = 0(rad)$, respectively, and the simulation duration is 800 seconds.

TABLE 2. Model parameters.

Parameter	Value	Parameter	Value
$Ix(kg/m^2)$	0.177	$K_{\dot{p}}(kg/m^2)$	-0.0704
$Iy(kg/m^2)$	3.45	$M_{\dot{q}}(kg/m^2)$	-4.880
$Iz(kg/m^2)$	3.45	$N_{\dot{r}}(kg/m^2)$	-4.880
$m(kg)$	30.48	$X_u(kg/s)$	-13.50
$B(N)$	299	$Y_v(kg/s)$	-44.96
$z_B(m)$	0.0196	$Z_w(kg/s)$	-66.60
$X_{\dot{u}}(kg)$	-35.50	$K_p(m^2/s)$	-19.54
$Y_{\dot{v}}\ (kg)$	-0.93	$M_q(m^2/s)$	-6.87
$Z_{\dot{w}}\ (kg)$	-35.50	$N_r(m^2/s)$	-76.82

Fig. 3 shows the trajectory of the QUV tracking of the desired position in the ζ direction, and Fig. 4 shows the ζ error value of the trajectory tracking. From these figures above, it can be determined that when the desired position changes, it takes approximately 2 seconds to reach the given position and then remain stable. In fact, when the output is not limited, the larger the output value, the shorter the time for the QUV to reach the desired value. The specific time to stabilize is related to the actual output of the QUV. In general, depth control is rapid and accurate.

B. HELIX CURVE TRACKING

This section demonstrates the efficacy and precision of NITSMC in a representative helix curve 3D trajectory. Moreover, in this experiment the control method is compared with the backstepping method to reveal the former's advantages.

$$\begin{cases} \xi_d = 10\sin(0.01t) \\ \eta_d = 10\cos(0.01t) \\ \zeta_d = 0.3t \end{cases} \tag{39}$$

The initial motion states of QUV are $u_0 = 0(m/s)$, $v_0 = 0(m/s)$, $w_0 = 0(m/s)$, $p_0 = 0(rad/s)$ and $q_0 = 0(rad/s)$. The initial position and angle are $\xi_0 = 0(m)$ $\eta_0 = 8(m)$ $\zeta_0 = 0(m)$ $\phi_0 = 0(rad)$ and $\theta_0 = 0.3(rad)$, respectively, and the simulation duration is 800 seconds.

Fig. 5 is the 3D helix curve trajectory of the QUV, where the black line is the desired trajectory, the blue line is the actual trajectory of the QUV with NITSMC, and the red line is the actual trajectory of the QUV with backstepping control.

Fig. 6 illustrates the projections of the actual and predefined desired QUV trajectory in the three directions of ξ, η, and ζ. Apparently, both BSC and NITSMC can successfully

$$\begin{aligned} \dot{V}_s &= s_1\left\{e_{w2} + \frac{1}{\beta_1}\frac{a_1}{b_1}e_{w2}^{a_1/b_1-1}(\dot{w}-\dot{\alpha}_w)\right\} + s_2\left\{e_{p2} + \frac{1}{\beta_2}\frac{a_2}{b_2}e_{p2}^{a_2/b_2-1}(\dot{p}-\dot{\alpha}_p)\right\} + s_3\left\{e_{q2} + \frac{1}{\beta_3}\frac{a_3}{b_3}e_{q2}^{a_3/b_3-1}(\dot{q}-\dot{\alpha}_q)\right\} \\ &= s_1\left\{e_{w2} + \frac{1}{\beta_1}\frac{a_1}{b_1}e_{w2}^{a_1/b_1-1} \times \left(\frac{1}{m-Z_{\dot{w}}}\left(Z_w w + (m-X_{\dot{u}})qu - (m-Y_v)pv + c\phi c\theta(B-W) + U_1\right)\right)\right\} \\ &\quad + s_2\left\{e_{p2} + \frac{1}{\beta_2}\frac{a_2}{b_2}e_{p2}^{a_2/b_2-1} \times \left(\frac{1}{I_x-K_{\dot{p}}}\left(K_p p - (Y_{\dot{v}}+Z_{\dot{w}})vw - Bz_B c\theta s\phi + U_2\right)\right)\right\} \\ &\quad + s_3\left\{e_{q2} + \frac{1}{\beta_3}\frac{a_3}{b_3}e_{w2}^{a_3/b_3-1} \times \left(\frac{1}{I_y-M_{\dot{q}}}\left(M_q q + (X_{\dot{u}}+Z_{\dot{w}})uw - Bz_B s\theta + U_3\right)\right)\right\} \end{aligned} \tag{32}$$

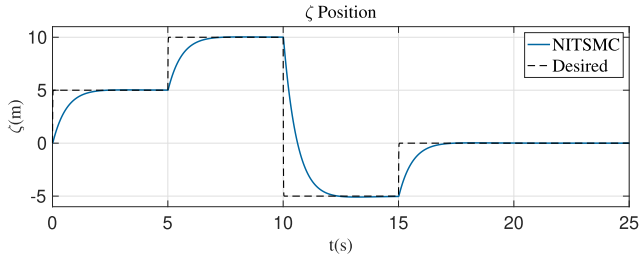

FIGURE 3. Depth tracking.

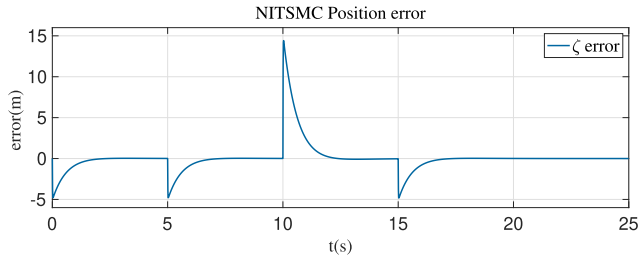

FIGURE 4. Depth tracking error.

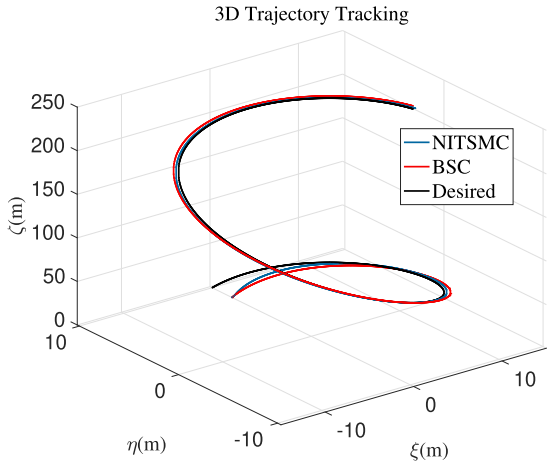

FIGURE 5. 3D view of the trajectory.

drive QUV to track the desired curve. At the initial moment, the QUV is right on the desired trajectory in both the ξ and ζ directions; therefore, it always follows the trajectory and keeps the error within a small range. However, there is a large error at the initial moment in the η direction. It is obvious that QUV with NITSMC is faster at reaching the trajectory. The convergence times of the η tracking error for the NITSMC and BSC methods are approximately 100 s and 120 s, respectively.

Fig. 7 refers to the response curve of the QUV tracking position error based on each method. After the QUV runs stably (approximately 100 s), for the control method based on NITSM, the errors in the 3 directions remain in $[-0.28, 0.28]$, $[-0.07, 0.07]$ and $[0, 0.05]$, respectively, and for the control method based on BSC, the errors in the 3 directions remain in $[-0.50, 0.46]$, $[-0.49, 0.46]$ and $[0, 0.17]$, respectively.

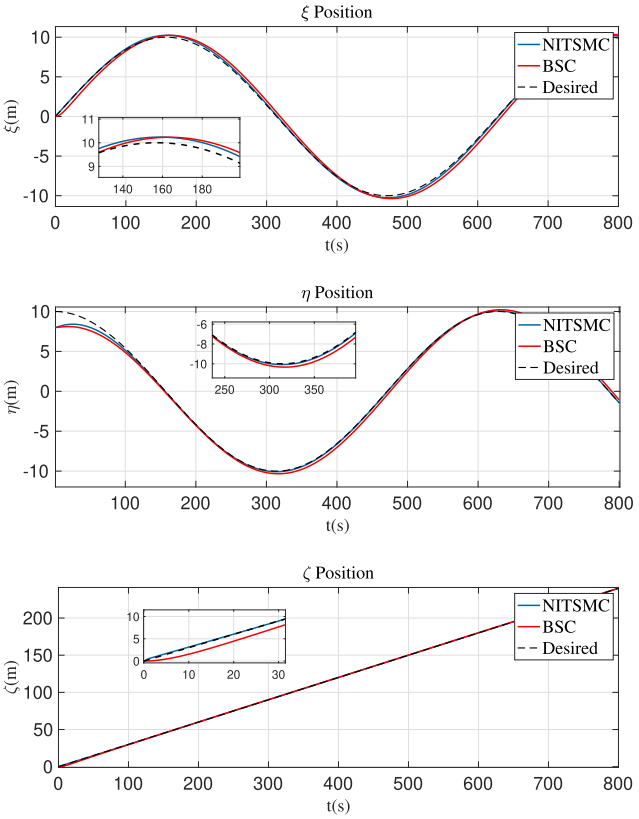

FIGURE 6. Helix curve tracking.

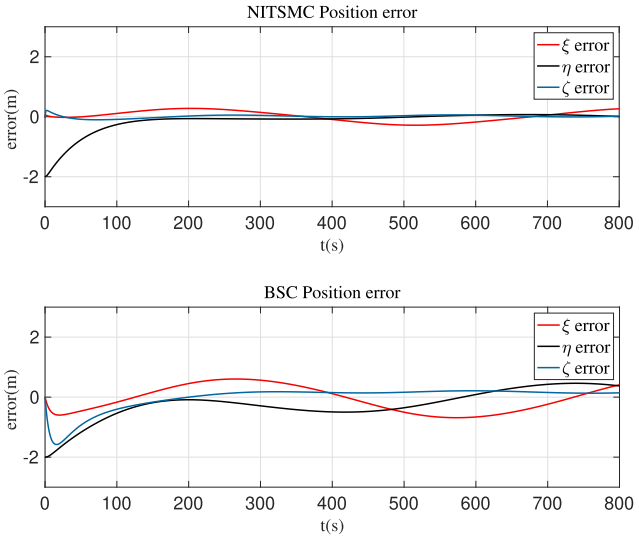

FIGURE 7. Tracking error.

In addition, the error in the ξ direction is slightly larger than that in the other two directions at the turning point of the trajectory, which is related to the parameters of the model.

Fig. 8 shows the values of ϕ and θ and the expected ϕ_d and θ_d during the trajectory tracking of the vehicle. In the initial stage, the ϕ angle drastically changes to a negative value because the QUV needs to move closer to the expected

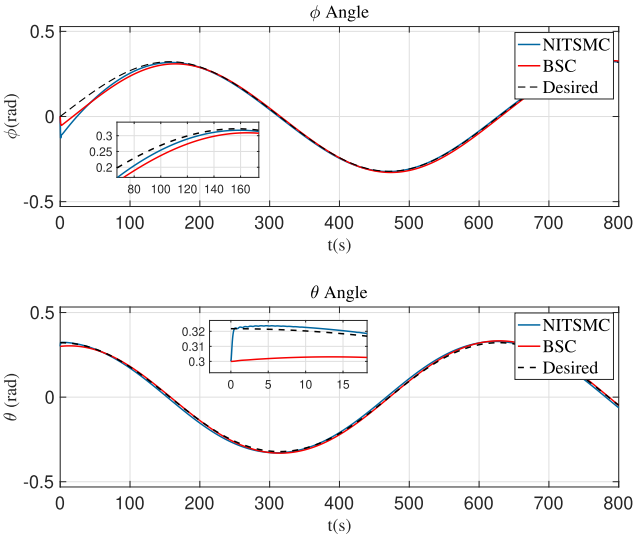

FIGURE 8. ϕ angle and θ angle tracking.

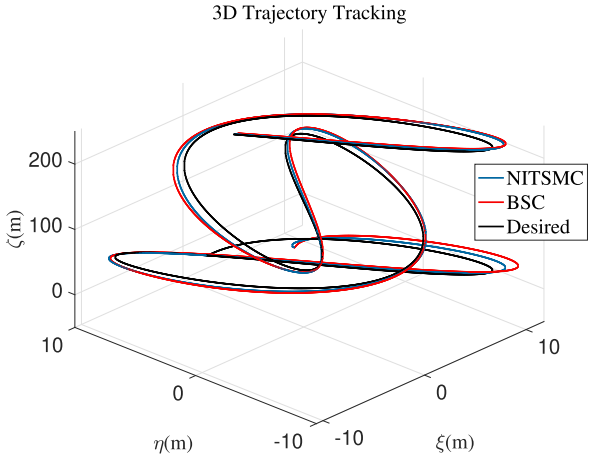

FIGURE 9. 3D trajectory.

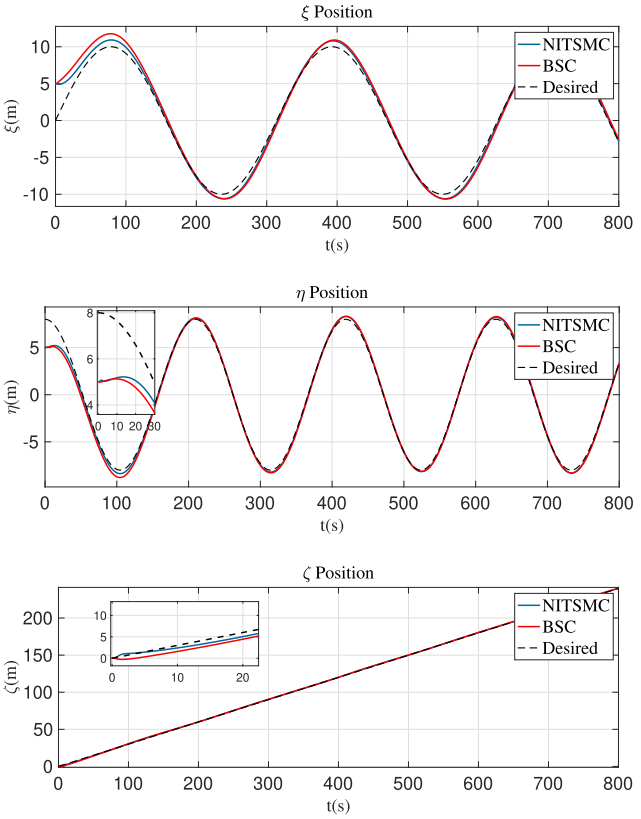

FIGURE 10. Aggressive curve tracking.

value in the η direction, forcing the body to rotate around the X axis of the body frame by a negative angle ϕ. With the help of NITSMC, ϕ changes back to ϕ_d and quickly converges to the expected value and is faster than BSC. For angle θ, the rapidity of BSC is obviously slower than that of NITSMC. Throughout the whole tracking process, ϕ_{max} is $0.324(rad)$, ϕ_{min} is $-0.324(rad)$, θ_{max} is $0.329(rad)$, and θ_{min} is $-0.330(rad)$, which are all within the small angle range that the QUV can accept.

C. AGGRESSIVE CURVE TRACKING

We selected another more adventurous tracking trajectory to test the robustness of the control method. The spatial trajectory setting is as follow:

$$\begin{cases} \xi_d = 10\sin(0.02t) \\ \eta_d = 8\cos(0.03t) \\ \zeta_d = 0.3t \end{cases} \tag{40}$$

The initial motion states of QUV are $u_0 = 0(m/s)$, $v_0 = 0(m/s)$, $w_0 = 0(m/s)$, $p_0 = 0(rad/s)$ and $q_0 = 0(rad/s)$. The initial position and angle are $\xi_0 = 5(m)$, $\eta_0 = 5(m)$, $\zeta_0 = 0(m)$, $\phi_0 = 0(rad)$ and $\theta_0 = 0(rad)$, respectively, and the simulation duration is 800 seconds.

Fig. 9 is the spatial curve trajectory of the QUV, where the black line is the desired trajectory, the red line is the actual trajectory of the QUV with backstepping control, and the blue line is the actual trajectory of QUV with NITSMC.

Fig. 10 illustrates the projections of the actual and predefined desired QUV trajectory in the three directions of ξ, η, and ζ. It can clearly be seen that both control methods can enforce vehicles to track the predefined trajectory with a rapid speed. Due to NITSMC's advantages, QUV responds quickly, and its trajectory is closer to the desired trajectory.

Fig. 11 refers to the response curve of the QUV tracking position error based on each method. In the first 100 s, it is obvious that the NITSMC error converges more quickly than that of BSC. After the QUV runs stably (approximately 100 s), for the control method based on NITSM, the error in 3 directions remains at $[-0.81, 0.83]$, $[-0.31, 0.30]$ and $[-0.01, 0.43]$, respectively, and for the control method based on BSC, the error in 3 directions remains at $[-1.04, 1.02]$, $[-0.34, 0.34]$ and $[0, 0.64]$, respectively.

Fig. 12 shows the relationship between the angle of the QUV movement and the desired value. The initial detailed part of the angle change is shown through a partially

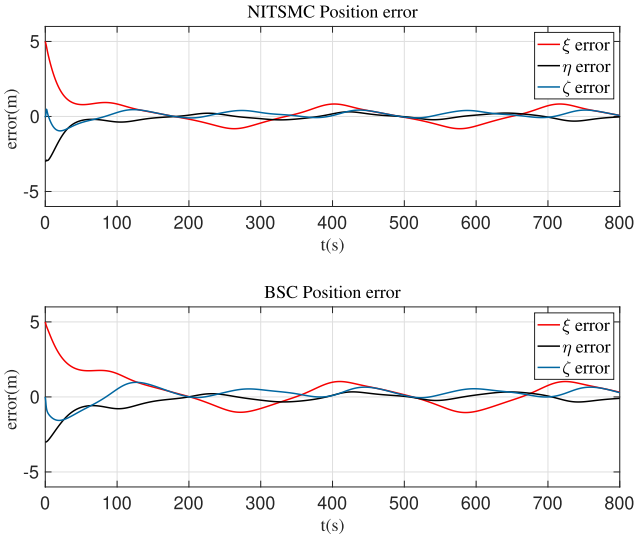

FIGURE 11. Tracking error.

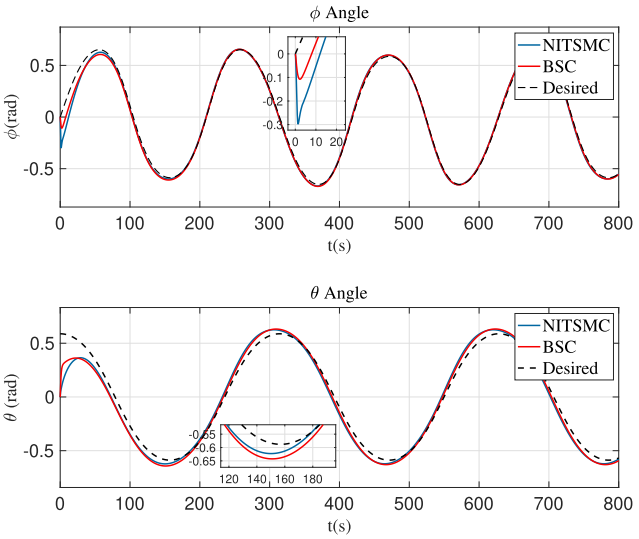

FIGURE 12. ϕ angle and θ angle tracking.

enlarged view. It can be observed that the initial ϕ drops sharply from 0 to a negative angle. This is because $\eta_0 = 5$ but $\eta_{d0} = 10$, so the QUV must rotate a negative angle around the X axis in the body frame to move in the negative direction of η. Similarly, with the initial $\xi = 5$ and $xi_{d0} = 8$, the QUV must rotate around the Y axis at a positive angle to chase the desired value. In the entire tracking process, ϕ_{max} is $0.670(rad)$, ϕ_{min} is $-0.670(rad)$, θ_{max} is $0.630(rad)$, and θ_{min} is $-0.635(rad)$, which are all close to the limit where the QUV can move.

Regardless of the kind of curve given, the NITSMC method has a shorter convergence time in terms of velocity and position tracking than the BSC method. In general, according to the simulation results and compared with BSC, we may safely draw the conclusion that the nonsingular integral terminal sliding mode method can realize the control of QUV trajectory tracking in a finite amount of time, with a high control quality and good robustness.

V. CONCLUSION AND FUTURE WORK

To solve the trajectory tracking control problem of an underactuated underwater vehicle with a new structure, this paper first established a 5-DOF kinematic and dynamic model of the QUV. Then, a controller with a double-loop structure was designed. According to three positions and two angle errors in the earth frame, a Lyapunov function was designed to obtain the virtual control law of the desired angular velocity α_w, α_p and α_q. The inner loop controller enables the angle velocity track to the specified value by designing the non-sigular integral terminal sliding mode control so that the overall position of the QUV tracks the desired trajectory. Finally, through a series of simulation experiments that included vertical depth control and three-dimensional curve trajectory with the NITSMC and BSC methods, the effectiveness and robustness of the control method were verified.

In terms of future work, the controller design part of this paper does not consider underwater environment interference or parameter perturbation issues. Thus, the influence of environmental resistance will be taken into consideration in our next stage of work. Furthermore, the model parameters of the QUV need to be determined accurately via computational fluid dynamics tools or experiments; however, Nan *et al.* proposed a new data-driven adaptive predictive control method to control unknown autonomous underwater vehicles [27] when the parameters are difficult to determine. Additionally, the propeller mathematical modeling part is not considered in this paper, and we ideally assume that the input is unrestricted without a dead zone. Yang *et al.* provided an effective method that considers handling of the actuator's dead zone [28]. It is essential to focus on this practical issue.

REFERENCES

[1] J. G. Bellingham, C. A. Goudey, T. R. Consi, J. W. Bales, D. K. Atwood, J. J. Leonard, and C. Chryssostomidis, "A second generation survey AUV," in *Proc. IEEE Symp. Auto. Underwater Vehicle Technol. (AUV94)*, 1994.

[2] B. Allen, R. Stokey, T. Austin, N. Forrester, R. Goldsborough, M. Purcell, and C. von Alt, "REMUS: A small, low cost AUV; system description, field trials and performance results," in *Proc. MTS/IEEE Conf.*, vol. 2, Oct. 1997, pp. 994–1000.

[3] D. R. Yoerger, J. Newman, and J.-J. E. Slotine, "Supervisory control system for the JASON ROV," *IEEE J. Ocean. Eng.*, vol. 11, no. 3, pp. 392–400, Jul. 1986.

[4] P. L. J. Drews, A. A. Neto, and M. F. M. Campos, "Hybrid unmanned aerial underwater vehicle: Modeling and simulation," in *Proc. IEEE/RSJ Int. Conf. Intell. Robots Syst.*, Sep. 2014, pp. 4637–4642.

[5] T. Ranganathan, A. Thondiyath, and S. P. S. Kumar, "Design and analysis of an underwater quadrotor–AQUAD," in *Proc. IEEE Underwater Technol. (UT)*, Feb. 2015, pp. 1–5.

[6] D. Qi, J. Feng, A. Liu, J. Hu, H. Xu, Y. Li, and M. A. Ashraf, "Stability control of propeller autonomous underwater vehicle based on combined sections method," *Polish Maritime Res.*, vol. 22, no. s1, pp. 157–162, Sep. 2015.

[7] J. Bian, "Design and key technologies for quadrotor unmanned underwater vehicle," M.S. thesis, College Elect. Eng., Zhejiang Univ., Hangzhou, China, 2019.

[8] P. Encarnacao and A. Pascoal, "3D path following for autonomous underwater vehicle," in *Proc. 39th IEEE Conf. Decis. Control*, vol. 3, Dec. 2000, pp. 2977–2982.

[9] L. Lapierre, D. Soetanto, and A. Pascoal, "Nonlinear path following with applications to the control of autonomous underwater vehicles," in *Proc. 42nd IEEE Int. Conf. Decis. Control*, vol. 2, Dec. 2003, pp. 1256–1261.
[10] K. D. Do and P. Jie, *Control Ships Underwater Vehicles*, 2009th ed. New York, NY, USA: Springer, Aug. 2009.
[11] F. Repoulias and E. Papadopoulos, "Planar trajectory planning and tracking control design for underactuated AUVs," *Ocean Eng.*, vol. 34, nos. 11–12, pp. 1650–1667, Aug. 2007.
[12] J. Li, H. Guo, H. Zhang, and Z. Yan, "Double-loop structure integral sliding mode control for UUV trajectory tracking," *IEEE Access*, vol. 7, pp. 101620–101632, 2019.
[13] Y. Jiang, C. Guo, and H. Yu, "Robust trajectory tracking control for an underactuated autonomous underwater vehicle based on bioinspired neurodynamics," *Int. J. Adv. Robotic Syst.*, vol. 15, no. 5, 2018, Art. no. 1729881418806745.
[14] S. Vahid and K. Javanmard, "Modeling and control of autonomous underwater vehicle (AUV) in heading and depth attitude via PPD controller with state feedback," in *Proc. 18th Mar. Industries Conf. (MIC)*, 2016, pp. 11–18.
[15] C. Yuan, R. Zhang, X. Zhao, and J. Gao, "Adaptive fuzzy inverse trajectory tracking control of underactuated underwater vehicle with uncertainties," *Ocean Eng.*, vol. 121, pp. 123–133, Jul. 2016.
[16] S. Heshmati-Alamdari, A. Nikou, and D. V. Dimarogonas, "Robust trajectory tracking control for underactuated autonomous underwater vehicles in uncertain environments," *IEEE Trans. Autom. Sci. Eng.*, vol. 18, no. 3, pp. 1288–1301, Jul. 2021.
[17] H. Zhao and D. Zhu, "UUV trajectory tracking control with fault tolerant based on MPC," in *Proc. Chin. Control Decis. Conf. (CCDC)*, Aug. 2020, pp. 2403–2408.
[18] L. Qiao and W. Zhang, "Double-loop integral terminal sliding mode tracking control for UUVs with adaptive dynamic compensation of uncertainties and disturbances," *IEEE J. Ocean. Eng.*, vol. 44, no. 1, pp. 29–53, Jan. 2019.
[19] T. I. Fossen, *Marine Control Systems Guidance, Navigation, and Control of Ships, Rigs and Underwater Vehicles*, Trondheim, Norway: Marine Cybernetics, 2002, ch. 2, pp. 29–155.
[20] T. I. Fossen, "Mathematical models of ships and underwater vehicles," in *Encyclopedia of Systems and Control*. London, U.K.: Springer, 2014, pp. 6–9.
[21] H. C. T. E. Fernando, A. T. A. De Silva, M. D. C. De Zoysa, K. A. D. C. Dilshan, and S. R. Munasinghe, "Modelling, simulation and implementation of a quadrotor UAV," in *Proc. IEEE 8th Int. Conf. Ind. Inf. Syst.*, Dec. 2013, pp. 207–212.
[22] J. Liu, *Sliding Mode Control Design and MATLAB Simulation*. Beijing, China: Tsinghua Univ. Press, 2019.
[23] L. Qiao and W. Zhang, "Adaptive non-singular integral terminal sliding mode tracking control for autonomous underwater vehicles," *IET Control Theory Appl.*, vol. 11, no. 8, pp. 1293–1306, Feb. 2017.
[24] T. Prester, "Verification of a six-degree of freedom simulation model for the remus autonomous underwater vehicle," M.S. thesis, College Eng., Univ. California, Davis, CA, USA, 1994.
[25] Y. C. Yinpo Yan and F. Yu, "Hydrodynamic coefficients calculation and dynamic modeling of an open-frame underwater robot," *Acta Armamentarii*, vol. 3, no. 4, pp. 1–15, May 2021.
[26] Q. Yin, "Path following control of the underactuated auv based on backstepping sliding mode," M.S. thesis, Nav. Archit. Ocean Eng. College, Dalian Maritime Univ., Dalian, China, 2016.
[27] D. Nan, Y. Weng, Y. Liu, and X. Wang, "Accurate trajectory tracking control of unknown autonomous underwater vehicles: A data-driven predictive approach," in *Proc. IEEE 10th Data Driven Control Learn. Syst. Conf. (DDCLS)*, May 2021, pp. 1241–1245.
[28] T. Yang, N. Sun, and Y. Fang, "Adaptive fuzzy control for a class of MIMO underactuated systems with plant uncertainties and actuator deadzones: Design and experiments," *IEEE Trans. Cybern.*, early access, Feb. 2, 2021, doi: 10.1109/TCYB.2021.3050475.

ZHIWEI WU was born in Fujian, China, in 2000. He is currently pursuing the bachelor's degree with the College of Information Science and Technology, Beijing University of Chemical Technology (BUCT), Beijing. His research interests include autonomous underwater vehicle control and mathematical modeling.

HAOSONG PENG was born in Sichuan, China, in 2000. He is currently pursuing the bachelor's degree with the College of Information Science and Technology, Beijing University of Chemical Technology (BUCT), Beijing. His research interests include autonomous underwater vehicle control and quadrotor UAVs.

BIAO HU received the B.Sc. degree in control science and engineering from the Harbin Institute of Technology, in 2010, the M.Sc. degree in control science and engineering from Tsinghua University, in 2013, and the Ph.D. degree from the Department of Computer Science and the Department of Informatics, Technische Universitäts M̈uchen, Germany, in 2017. He is currently an Associate Professor with the College of Information Science and Technology, Beijing University of Chemical Technology. His research interests include path planning of autonomous driving and OpenCL computing in heterogeneous systems.

XIAODONG FENG received the Ph.D. degree from the School of Engineering and Technology, China University of Geosciences, Beijing, China, in 2002. His research interests include advanced detection technology and intelligent control equipment, material defect detection by infrared thermal waves, ROV control systems, and UAV control systems.